Supporting Information

Vacancy-Induced Modulation on the Interface Properties of Au$_{25}$(SCH$_3$)$_{18}$ Nanoclusters Supported on Defective Graphene

Pan Zhu, Yuping Chen and Qing Tang*

School of Chemistry and Chemical Engineering, Chongqing Key Laboratory of Chemical Theory and Mechanism, Chongqing University, Chongqing 401331, China

*To whom correspondence should be addressed.

E-mail: qingtang@cqu.edu.cn
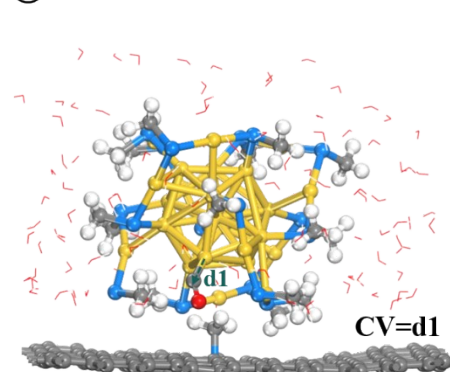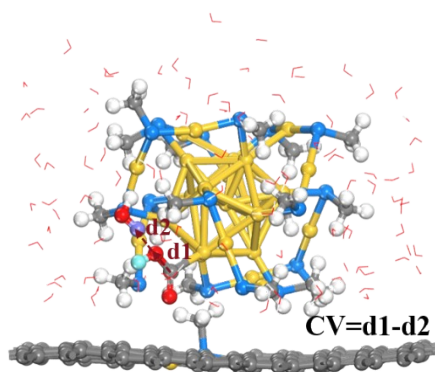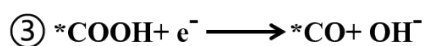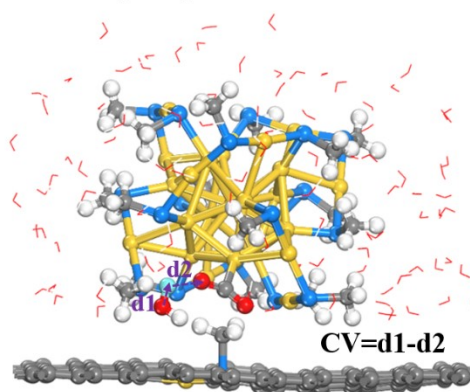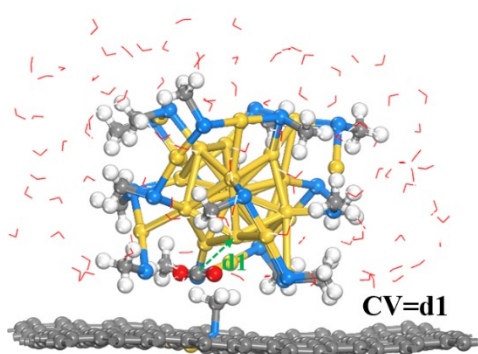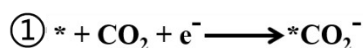
Figure S1. After performing AIMD simulation on Au$_{25}$-GV$_6$-1, the defined reaction collective variable (CV) for CO$_2$ reduction process (CO$_2$ activation, *CO$_2$ to *COOH, *COOH to *CO and CO desorption) in the system.
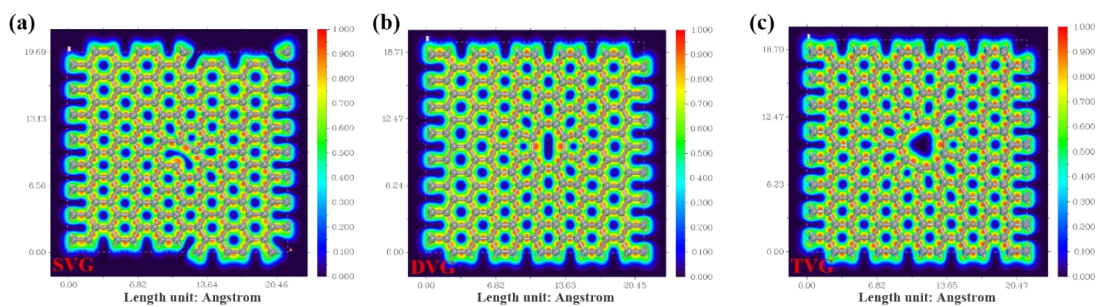
Figure S2. The ELF analysis on the electronic distribution of SVG (a), DVG (b), and TVG (c).
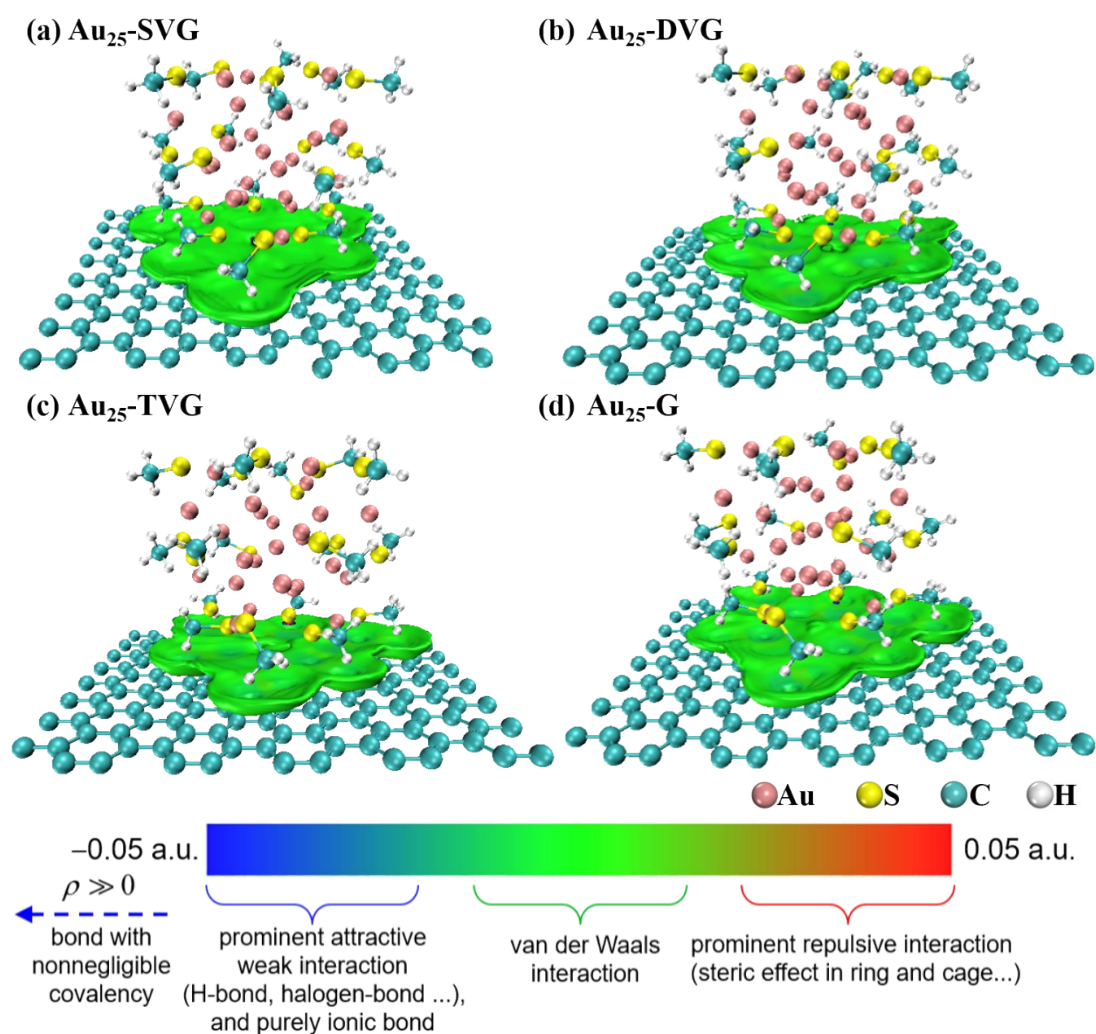
Figure S3. The IGMH method visualization reveals the weak interaction between Au_{25} and SVG (a), DVG (b), TVG (c), and pristine graphene (d).
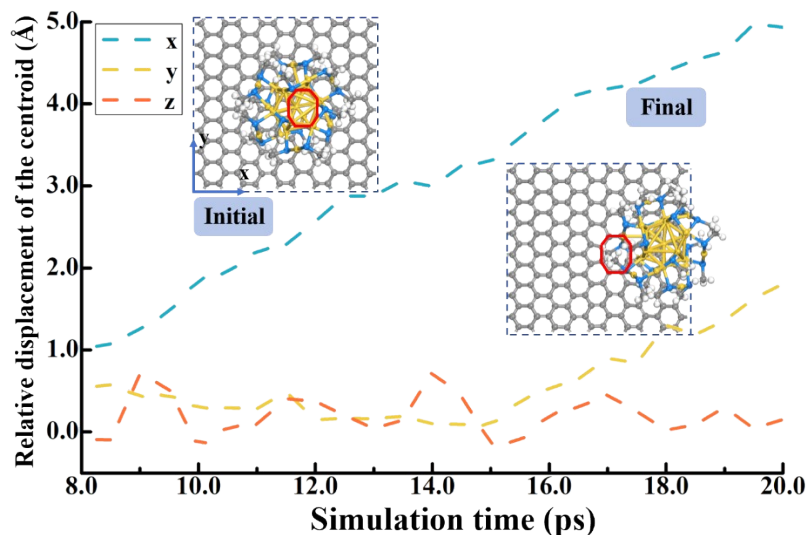
Figure S4. Displacement of Au$_{25}$ NC on DVG from 8ps to 20ps at 300 K along the direction of x, y, and z axes, respectively. The AIMD snapshots of the initial and final states are shown on the inset.
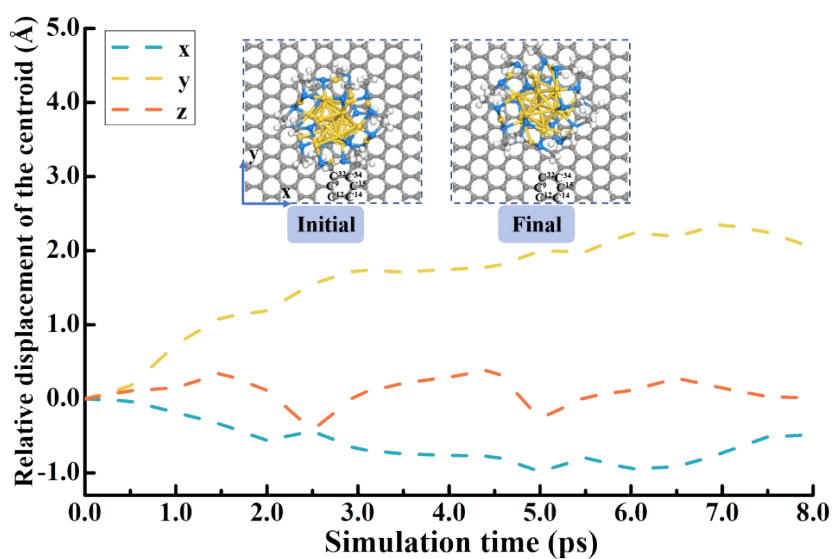
Figure S5. Displacement of Au$_{25}$ NC on the pristine graphene along the direction of x, y, and z axes, respectively. The AIMD snapshots of the initial and final states are shown inset.
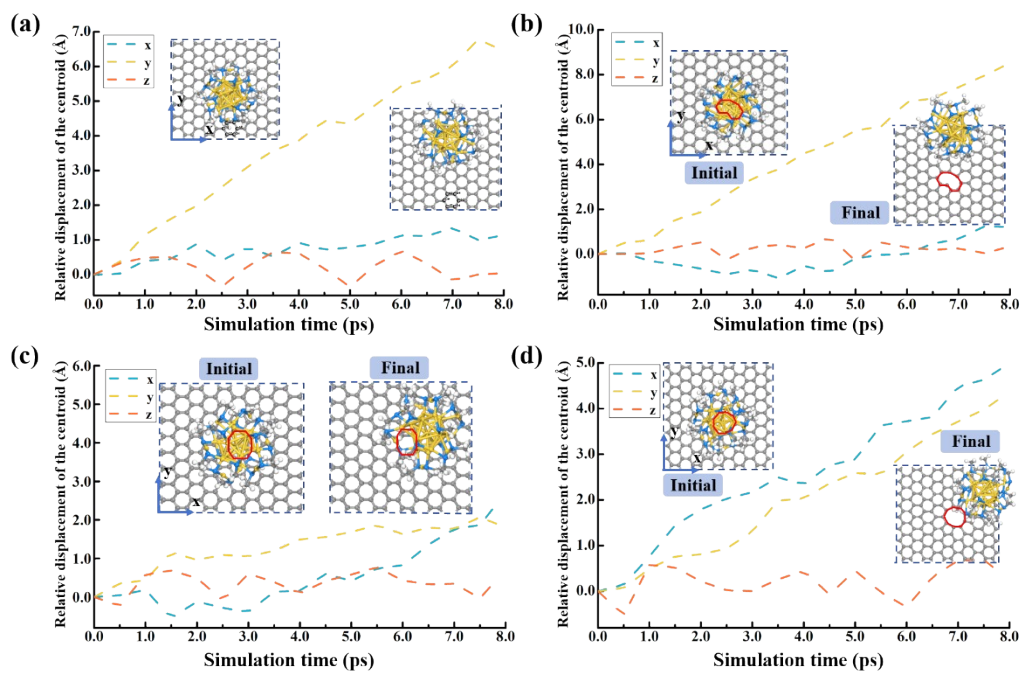
Figure S6. Displacement of Au$_{25}$ NC on pristine graphene (a), SVG (b), DVG (c), and TVG (d) along the direction of x, y, and z axes within 8ps AIMD simulations at 600K. The AIMD snapshots of the initial and final states are shown inset.
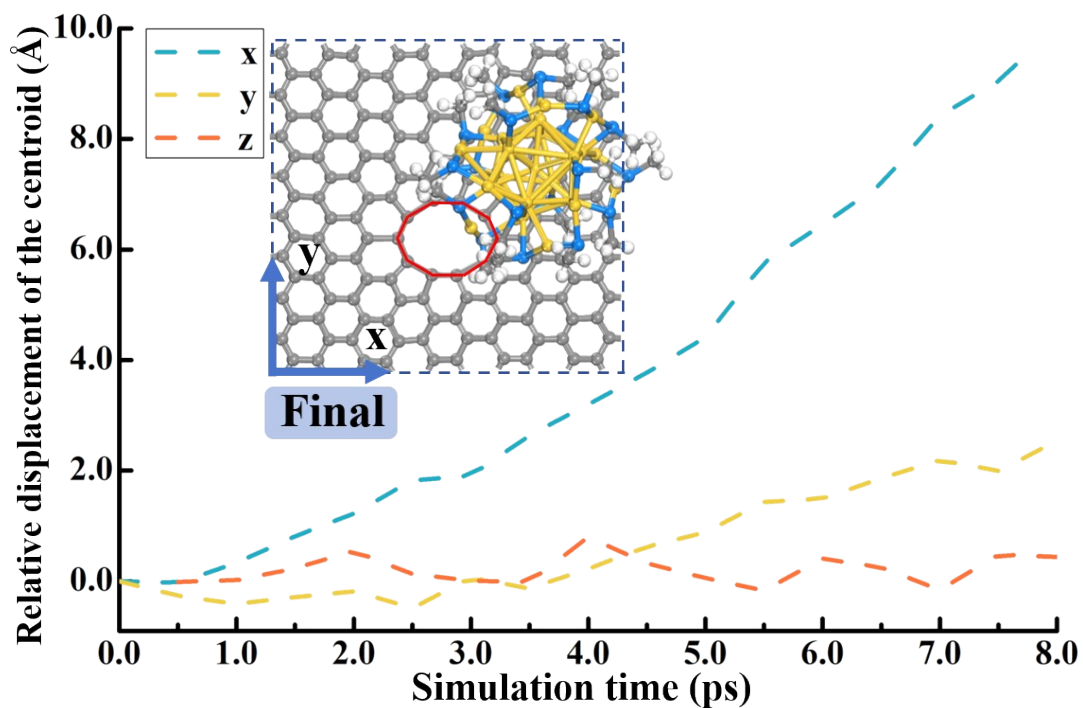
Figure S7. Displacement of Au$_{25}$ NC on GV$_6$-2 along the direction of x, y, and z axes at 600K. The AIMD snapshot of the final state after 8 ps simulations is shown inset.
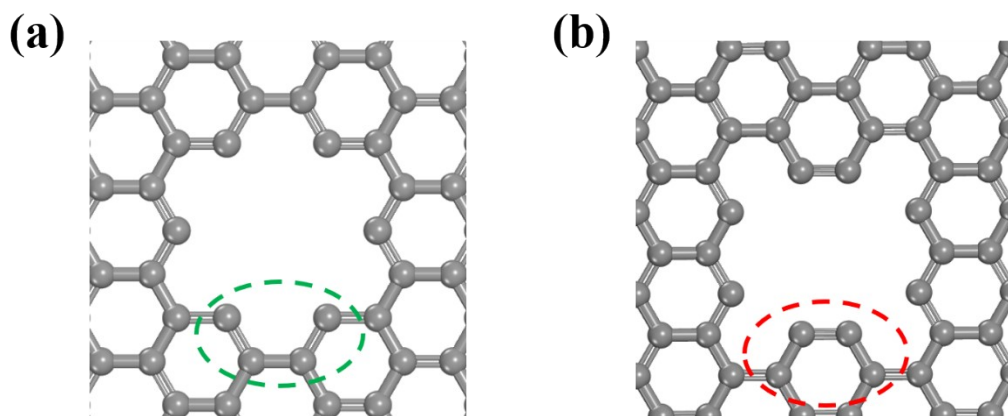
Figure S8. Vacancy edge structure of graphene substrates with six missing C atoms: initial structure of GV$_6$-1(a) and GV$_6$-2 (b).
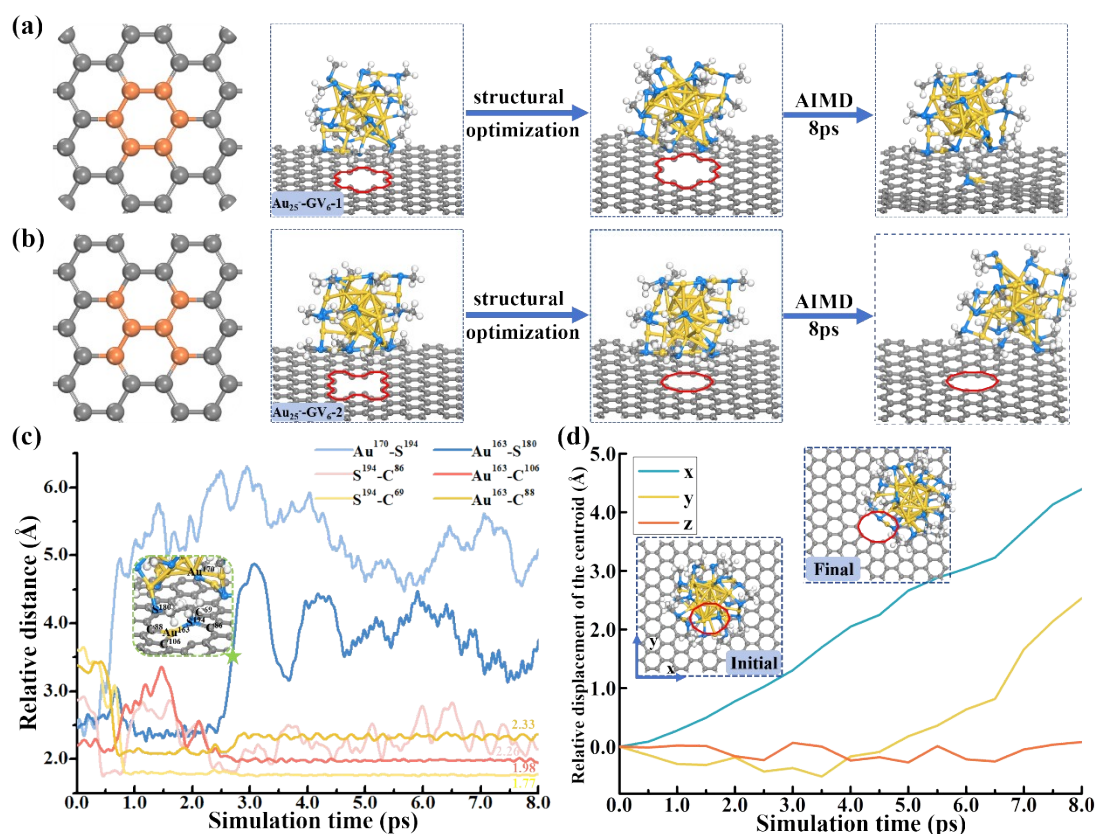
Figure S9. The structural model of Au$_{25}^-$ NC loaded on GV$_6$-1 (a) and GV$_6$-2 (b), displaying the optimized structure and the corresponding AIMD snapshots after 8ps simulations at 300K, the highlighted orange C atoms in the left column of (a) and (b) shows the six missing C sites in graphene. (c) Statistics of the relative distance between

the denoted key atoms during the equilibrated AIMD simulations of Au_{25}^--GV_6-1 system. (d) The displacement of Au_{25}^- NC on GV_6-2 along the x, y, and z axes, respectively, wherein the initial and final structures after 8ps AIMD simulations are shown inset.
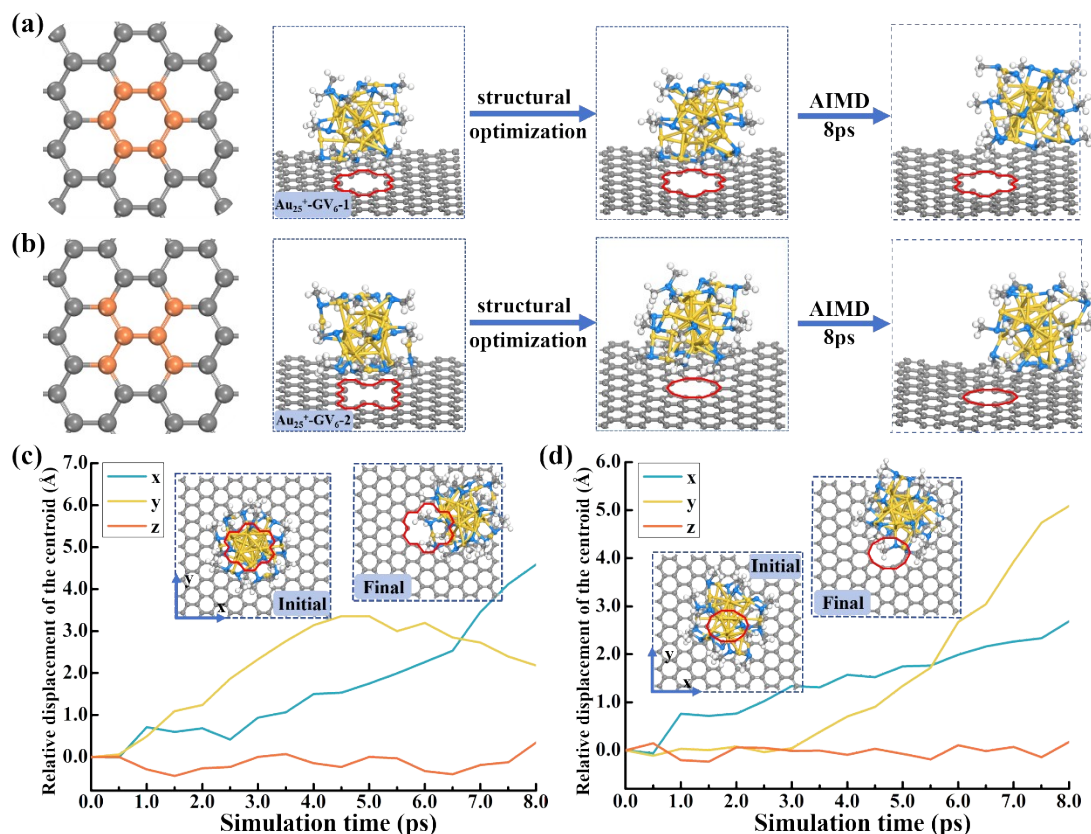
Figure S10. The structural model of Au_{25}^+ NC loaded on GV_6-1 (a) and GV_6-2 (b), displaying the optimized structure and the corresponding AIMD snapshots after 8ps simulations at 300K, the highlighted orange C atoms in the left column of (a) and (b) shows the six missing C sites in graphene. The displacement of Au_{25}^+ NC on (c) GV_6-1 and (d) GV_6-2 along the x, y, and z axes, respectively, wherein the initial and final structures after 8ps AIMD simulations are shown inset.
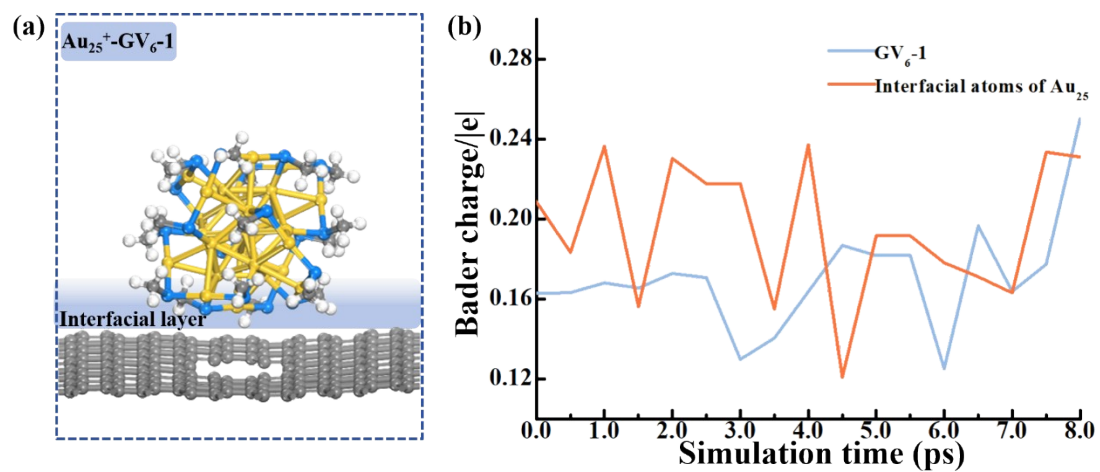
Figure S11. (a) The theoretical model of the Au_{25}^{+}-GV_6-1 system, where the blue-shaded region represents the interfacial layer of Au_{25}^{+}. (b) The charge distribution of the GV_6-1 substrate and the interfacial atoms of Au_{25}^{+} during equilibrium AIMD simulations.
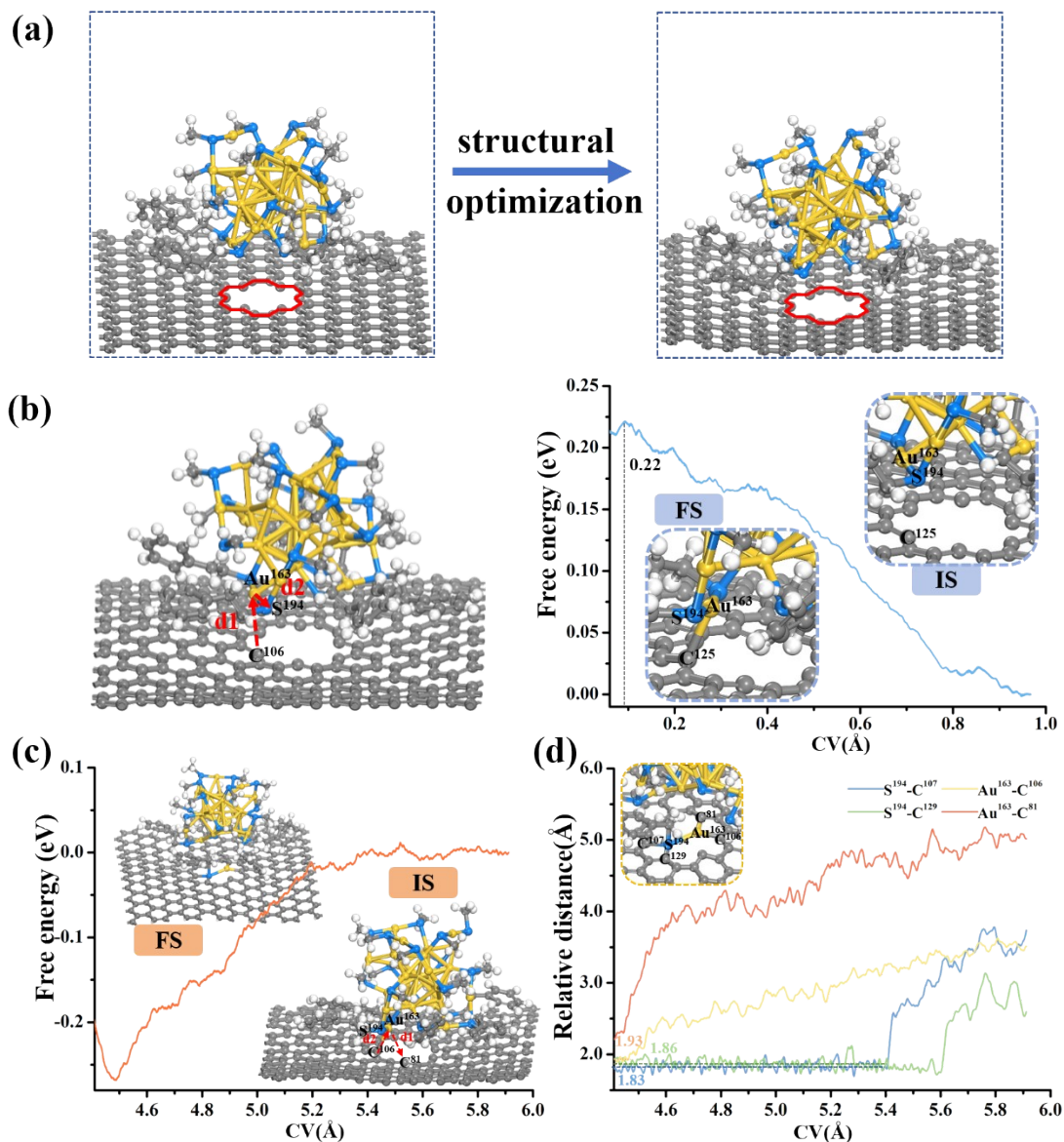
Figure S12. (a) The structural model of $Au_{25}(SR)_{18}$ (-SR at the interface is -SC_2H_4Ph) NC loaded on GV_6-1 and the optimized structure. (b) The integral free energy curve of Au_{25} approaching to GV_6-1. The collective variable (CV) is defined as d_1-d_2. (c) The integral free energy curve and (d) the relative distance between representative atoms for the removal of the Au-SR unit from Au_{25}. The collective variable (CV) is defined as d_1+d_2. IS and FS represent the initial and final structures.
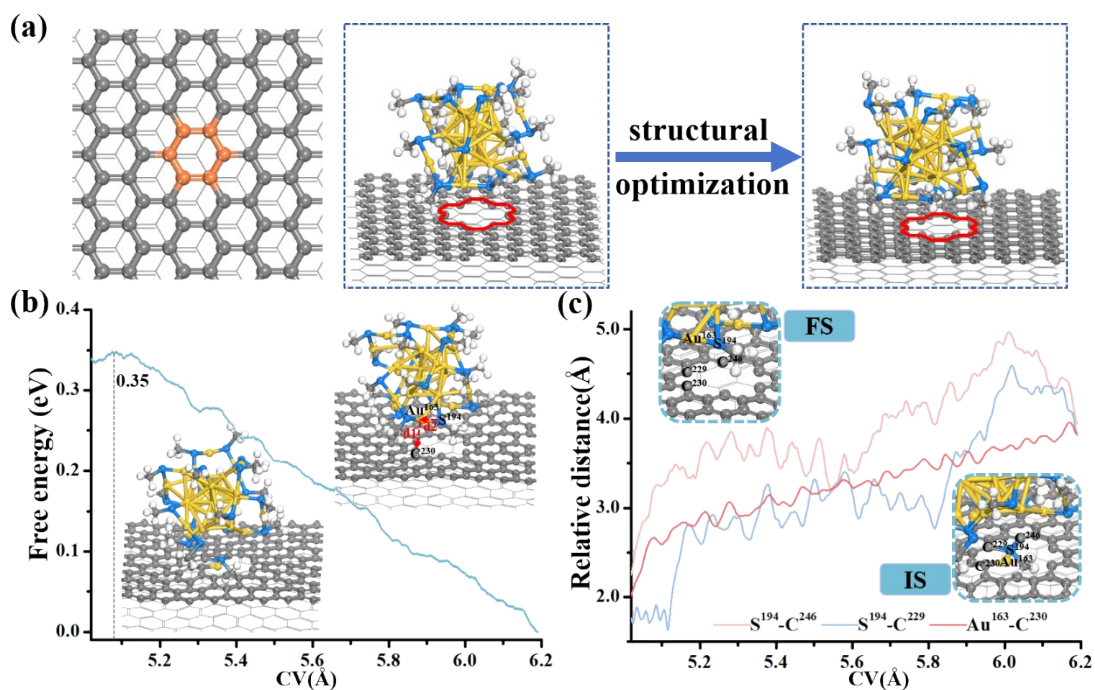
Figure S13. From left to right: the constructed bilayer graphene substrate with vacancy defects model (with the six removed C atoms shown in orange), the theoretical model of Au$_{25}$ NC loaded on substrate and the optimized structure. (b) The integral free energy curve and (c) the relative distance between representative atoms for the removal of the Au-SR unit from Au$_{25}$. The collective variable (CV) is defined as d$_1$+d$_2$. IS and FS represent the initial and final structures.
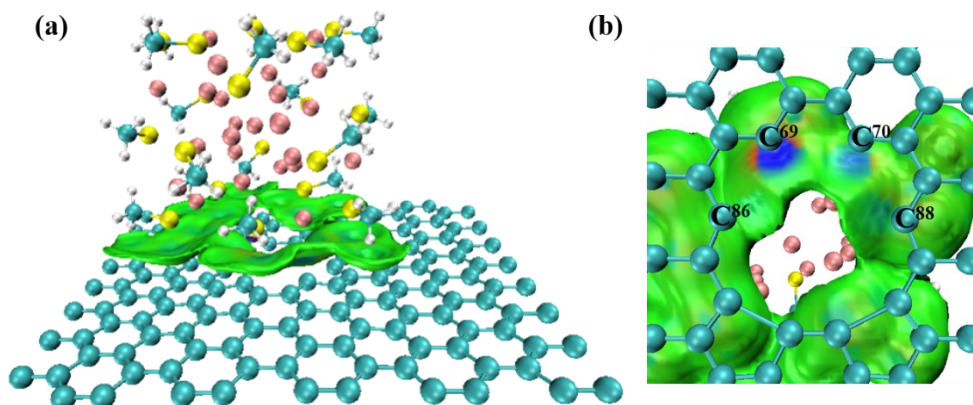
Figure S14. (a) The IGMH method visualization reveals the weak interaction between Au$_{25}$ and GV$_8$. (b) Local interaction of the interface atoms between Au$_{25}$ and the vacancy defect edges of GV$_8$.
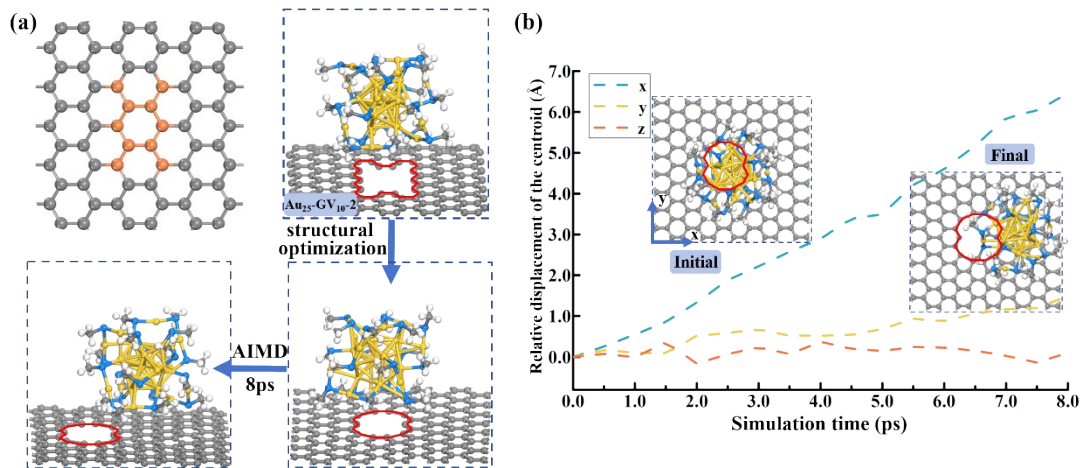
Figure S15. (a) The constructed GV_{10}-2 model (with the ten removed C atoms shown in orange), the theoretical model of Au_{25} NCs loaded on the GV_{10}-2 substrate, the optimized structure and the snapshot after 8ps AIMD simulations at 300K. (b) Displacement of Au_{25} NC on GV_{10}-2 along the x, y, and z axes at 300K, with the AIMD snapshots of the initial and final structures shown inset.
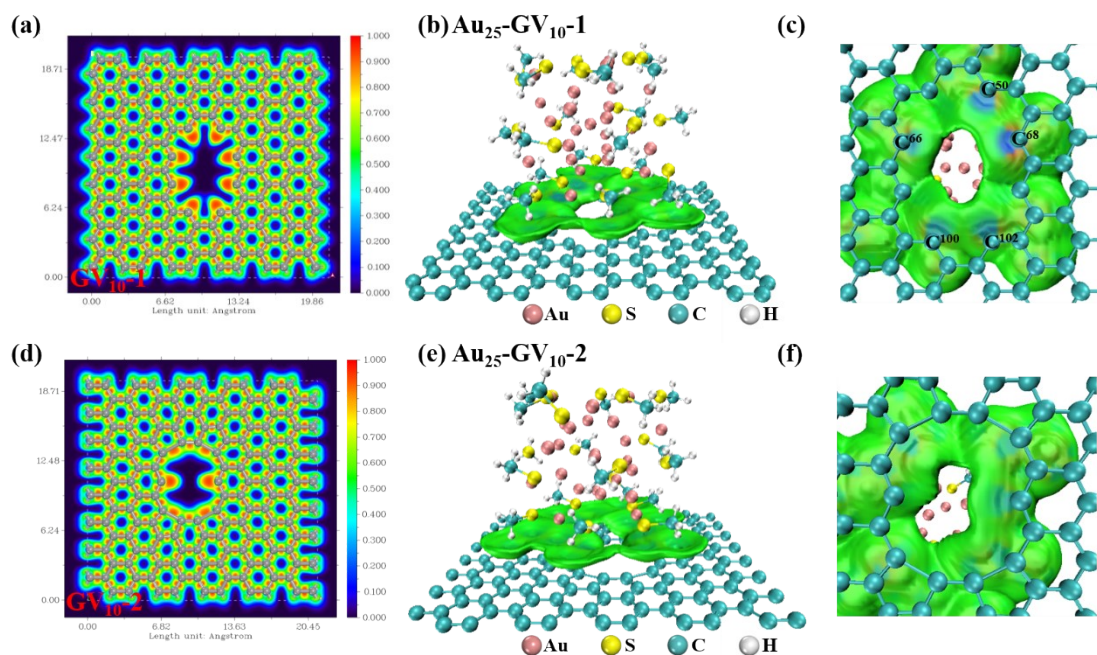
Figure S16. The ELF analysis on the electronic distribution of GV_{10}-1(a) and GV_{10}-2(d). The IGMH method visualization reveals the interactions between Au_{25} and GV_{10}-1(b) and GV_{10}-2(e). Local interaction of the interface atoms between Au_{25} and the vacancy defect edges of GV_{10}-1 (c) and GV_{10}-2 (f).
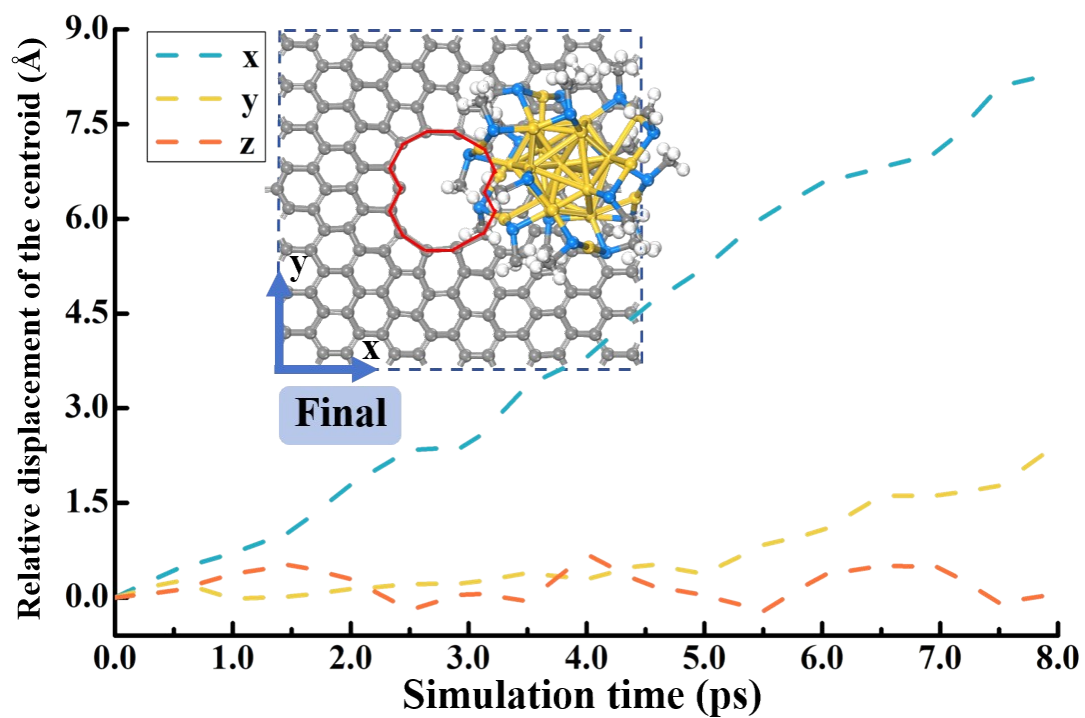
Figure S17. Displacement of Au_{25} NC on GV_{10}-2 along the direction of x, y, and z axes at 600K. The AIMD snapshot of the final state after 8 ps simulations is shown inset.
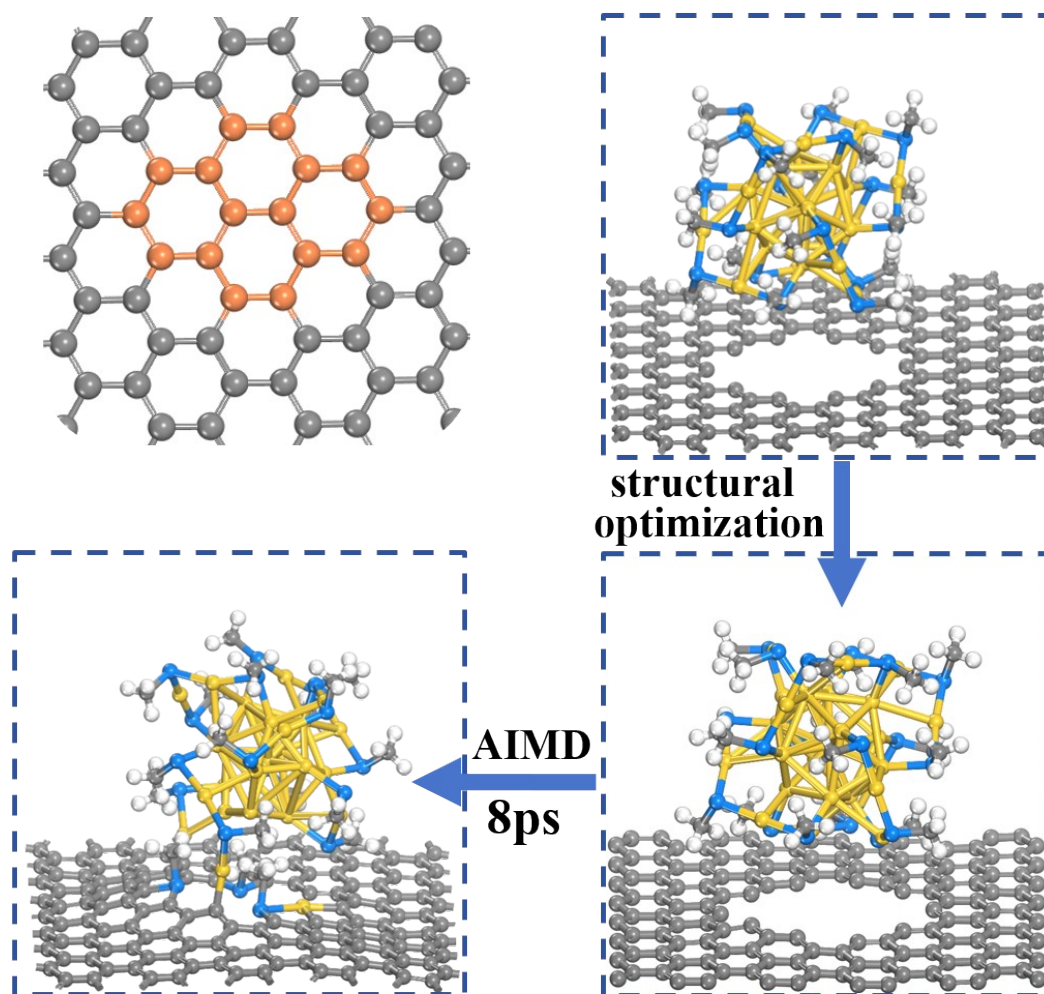
Figure S18. The constructed GV_{16} model (with the 16 removed C atoms shown in orange), the theoretical model of Au_{25} NCs loaded on the GV_{16} substrate, the optimized structure and the snapshot after 8ps AIMD simulations at 300K.

(a) standard Au$_{25}$

(b) Au$_{25}$-GV$_6$-1 in vacuum

Au$_{center}$ Au$_{surface}$ Au$_{staple}$ S
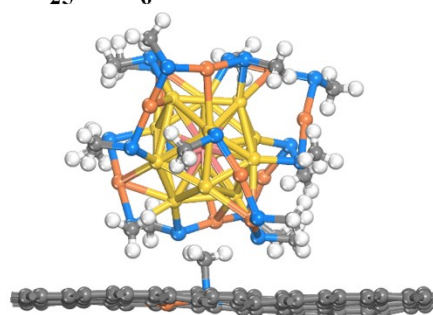
(c) Au$_{25}$-GV$_6$-1 in solution

(d) Au$_{25}$-GV$_6$-1 after CO desorption
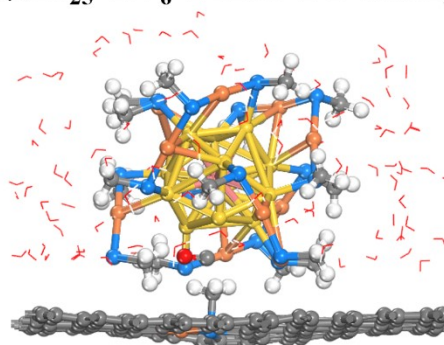
(e)

	standard Au$_{25}$	Au$_{25}$-GV$_6$-1 in vacuum	Au$_{25}$-GV$_6$-1 in solution	Au$_{25}$-GV$_6$-1 after CO desorption
Au$_{center}$-Au$_{surface}$	2.83	2.95	2.93	2.89
Au$_{surface}$-Au$_{surface}$	2.98	3.10	3.08	3.05
Au$_{surface}$-S	2.39	2.45	2.47	2.46
Au$_{staple}$-S	2.32	2.35	2.38	2.37

Figure S19. The structures of (a) standard Au$_{25}$, (b) Au$_{25}$-GV$_6$-1 in vacuum, (c) Au$_{25}$-GV$_6$-1 in solution and (d) Au$_{25}$-GV$_6$-1 after CO desorption as well as the average Au-Au bond lengths and Au-S bond lengths in the corresponding structures (e).
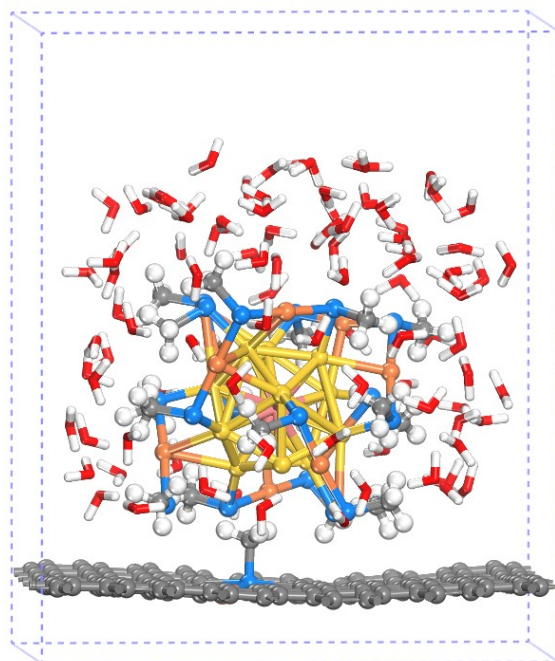
Figure S20. Schematic of the computational model containing etched Au_{25}-GV_6-1 system and 97 H_2O molecules. For clarity, all H_2O molecules are represented by stick modes.

Table S1. Bader charge analysis of Au atoms in Au_{25}-GV_6-1/water system after 8ps AIMD simulations at 300K.

atom	Charge	Net Charge
$Au^1_{surface}$	10.966	0.034
$Au^2_{surface}$	10.972	0.028
$Au^3_{surface}$	10.961	0.039

Au$^4_{surface}$	10.984	0.016
Au$^5_{surface}$	11.000	0.000
Au$^6_{staple}$	10.909	0.091
Au$^7_{staple}$	10.928	0.072
Au$^8_{staple}$	10.930	0.070
Au$^9_{staple}$	10.646	0.354
Au$^{10}_{surface}$	10.944	0.056
Au$^{11}_{staple}$	10.950	0.050
Au$^{12}_{staple}$	10.942	0.058
Au$^{13}_{surface}$	10.934	0.066
Au$^{14}_{suface}$	10.960	0.040
Au$^{15}_{surface}$	10.969	0.031
Au$^{16}_{surface}$	11.054	-0.054
Au$^{17}_{surface}$	10.972	0.028
Au$^{18}_{staple}$	10.956	0.044
Au$^{19}_{staple}$	10.907	0.093
Au$^{20}_{staple}$	10.866	0.134
Au$^{21}_{staple}$	10.869	0.131
Au$^{22}_{surface}$	10.938	0.062
Au$^{23}_{staple}$	10.935	0.065
Au$^{24}_{staple}$	10.923	0.077
Au$^{25}_{center}$	11.012	-0.012
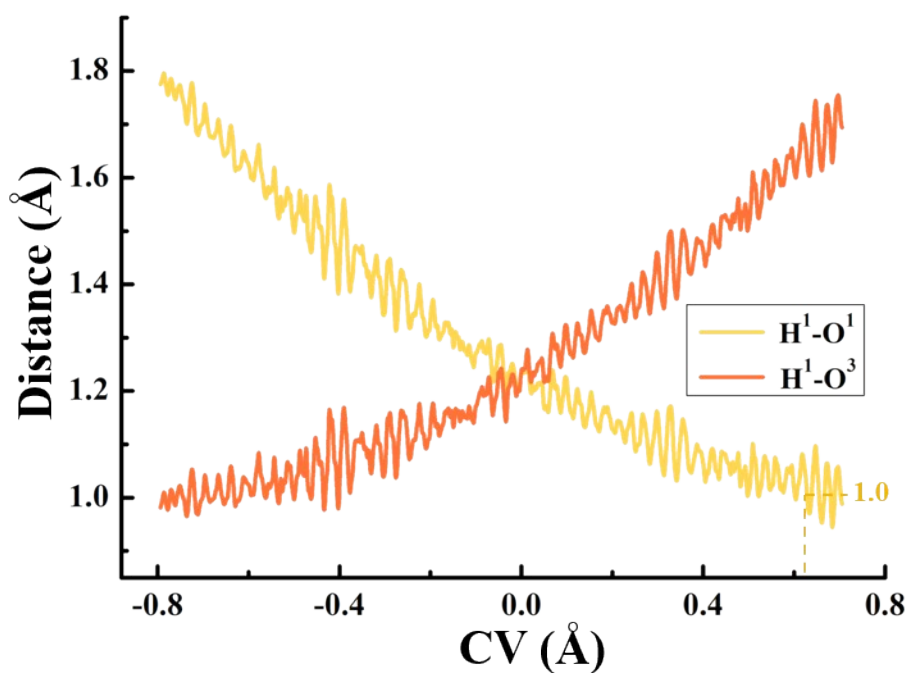
Figure S21. Critical H−O distances in H_2O molecules providing proton (orange line) and distance between the H of this H_2O and the O of $*CO_2$ (H−O, yellow line) during the *COOH formation.
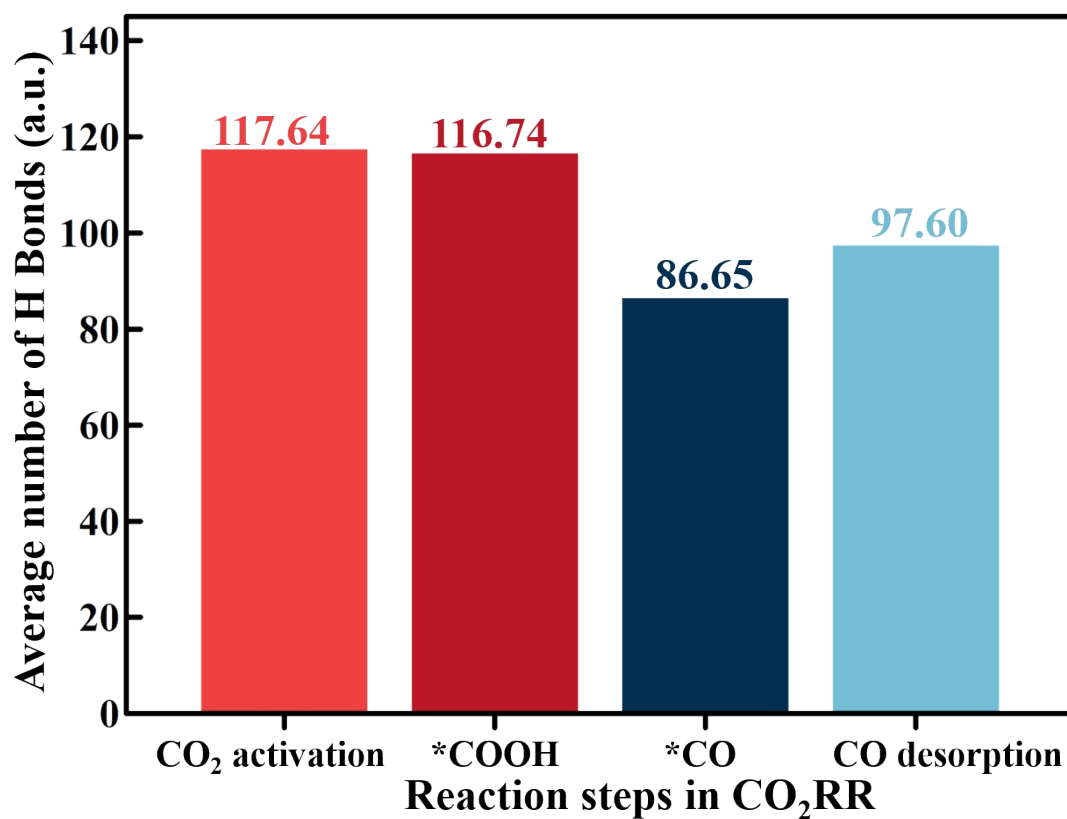
Figure S22. The number of hydrogen bonds for the etched Au_{25}-GV_6-1 system at different reaction steps of CO_2RR (*CO_2 activation, *COOH formation, *CO formation and CO desorption).